Available online at www.sciencedirect.com
ScienceDirect
International Journal of Multiphase Flow 34 (2008) 1008–1022
International Journal of Multiphase Flow
www.elsevier.com/locate/ijmulflow

Pool boiling heat transfer of ultra-light copper foam with open cells

Jinliang Xu [a,*], Xianbing Ji [a,b], Wei Zhang [a], Guohua Liu [a]

[a] Micro-Energy System Laboratory, Key Laboratory of Renewable and Gas Hydrate, Guangzhou Institute of Energy Conversion, Chinese Academy of Science, Guangzhou 510640, PR China
[b] Graduate School of Chinese Academy of Science, Beijing 100080, PR China

Received 12 December 2007; received in revised form 11 May 2008
Available online 6 June 2008

Abstract

High speed visualizations and thermal performance studies of pool boiling heat transfer on copper foam covers were performed at atmospheric pressure, with the heating surface area of 12.0 mm by 12.0 mm, using acetone as the working fluid. The foam covers have ppi (pores per inch) from 30 to 90, cover thickness from 2.0 to 5.0 mm, and porosity of 0.88 and 0.95. The surface superheats are from −20 to 190 K, and the heat fluxes reach 140 W/cm^2. The 30 and 60 ppi foam covers show the periodic single bubble generation and departure pattern at low surface superheats. With continuous increases in surface superheats, they show the periodic bubble coalescence and/or re-coalescence pattern. Cage bubbles were observed to be those with liquid filled inside and vented to the pool liquid. For the 90 ppi foam covers, the bubble coalescence takes place at low surface superheats. At moderate or large surface superheats, vapor fragments continuously escape to the pool liquid.

Boiling curves of copper foams show three distinct regions. Region I and II are those of natural convection heat transfer, and nucleate boiling heat transfer for all the foam covers. Region III is that of either a resistance to vapor release for the 30 and 60 ppi foam covers, or a capillary-assist liquid flow towards foam cells for the 90 ppi foam covers. The value of ppi has an important effect on the thermal performance. Boiling curves are crossed between the high and low ppi foam covers. Low ppi foams have better thermal performance at low surface superheats, but high ppi foams have better one at moderate or large surface superheats and extend the operation range of surface superheats. The effects of other factors such as pool liquid temperature, foam cover thickness on the thermal performance are also discussed.

Keywords: Copper foam; Pool boiling; Boiling pattern; Cage bubble; Boiling curve

1. Introduction

Compared with forced convection heat transfer, pool boiling heat transfer is a more attractive alternative scheme because it is generally less complex and easier to seal (Rainey and You, 2000). Enhancements in pool boiling heat transfer can be fulfilled by increasing the active nucleation sites and/or the bubble detaching frequency, which could decrease the surface superheat and increase the boiling heat flux (Parker and El-Genk, 2005). Honda and Wei (2004) gave a review on the enhanced boiling heat transfer from electronic components by use of surface micro-structures. The primary issues are the mitigation of incipience temperature overshoot, enhancement of nucleate boiling heat transfer and increasing the critical heat flux (CHF).

Rainey and You (2000) examined the pool boiling of a "double enhancement" technique which required a surface enhancement (micro-porous coating) and an extended area enhancement (square pin fins) using 1 cm^2 flush-mounted copper surfaces. An increase in surface roughness strongly increases the nucleate boiling heat transfer coefficient and critical heat flux, due to the increased active nucleation site density. It is believed that the presence of the pin fins produces a resistance to vapor bubble departure, which increases the bubble residence time and causes a change in the boiling curve slope of both plain and micro-porous finned surfaces.

* Corresponding author. Fax: +86 20 87057656.
E-mail address: xujl@ms.giec.ac.cn (J. Xu).

0301-9322/$ - see front matter © 2008 Elsevier Ltd. All rights reserved.
doi:10.1016/j.ijmultiphaseflow.2008.05.003

Modulated (periodically non-uniform thickness) porous-layer coatings, as shown by Liter and Kaviany (2001), can enhance the pool boiling critical heat flux nearly three times over that of a plain surface. The modulation separates the liquid and vapor phases, thus reducing the liquid–vapor counterflow resistance adjacent to the heated surface. Two independent mechanisms being capable of causing the liquid choking that leads to the critical heat flux were suggested.

Kim et al. (2002) investigated the mechanism of nucleate boiling heat transfer enhancement from micro-porous surfaces in saturated FC-72. The test section was a 390-μm diameter platinum wire coated with micro-porous particles. The nucleate boiling heat transfer is augmented through increased latent heat transfer in the low heat flux region and increased convection heat transfer in the high heat flux region.

Ghiu and Joshi (2005) visualized pool boiling from thin confined enhanced structure using a dielectric fluorocarbon liquid (PF 5060) as the working fluid at atmospheric pressure. Visualizations show the presence of two boiling regimes: slug predominance regime, slugs and plugs regime. Vapor slugs exist in the top and bottom channels even for lowest heat fluxes and exhibit an oscillatory movement, indicating the transient nature of internal evaporation.

Parker and El-Genk (2005) experimentally studied enhancements in nucleate boiling of FC-72 dielectric liquid on porous graphite and compared results with those on a smooth copper surface of the same size (10×10 mm). The surface temperature excursion at boiling incipience and critical heat fluxes are compared with those of other investigators on copper, silicon, micro-finned silicon surfaces and micro-porous coatings. It is shown that there is no temperature excursion at boiling incipience. Both the nucleate boiling heat transfer coefficients and critical heat fluxes are increased with increases in liquid subcooling.

Nimkar et al. (2006) studied pool boiling characteristics of pyramidal shaped re-entrant cavities etched in silicon. Experiments were performed in saturated FC-72 at atmospheric pressure. High speed visualization was performed to record and quantify the bubble departure frequency, the departure diameter, the active site density, and to observe the effect of interaction between neighboring nucleation sites.

Meléndez and Reyes (2006) performed enhancements in pool boiling heat transfer using iron wool and stainless steel wool with binary mixture as the working fluid. It is found that the combination of porous covers and positive binary mixture reduces the bubble size and coalescence, thus increases the liquid supply towards the heating surface, causing an increase in the convective heat transfer coefficient for pool boiling. For limited vapor-release conditions, the bubbles grow with no increase in heat transfer coefficient, while for resistance-free vapor escape the bubbles radii increase almost linearly.

The available studies of flow and heat transfer in porous media concern low porosity media such as packed beds and granular media, for which the porosity varies from 0.3 to 0.6. In the past several years, some studies were performed on the pool boiling heat transfer in metallic foams. Arbelaez et al. (2000) studied pool boiling of FC-72 in highly porous metal foam heat sinks. Experiments were conducted with samples of porosities and pore sizes in the range of 90–98% and 5–40 ppi, respectively. The results show that the temperature excursion usually observed for fluorinert fluids at the onset of nucleate boiling is not present. For the same pore size, the low porosity samples exhibit a significantly higher heat transfer coefficient in the low heat flux regimes. For similar porosity, enhanced heat transfer is observed with an increase in the value of ppi.

Athreya et al. (2002) investigated the effects of orientation and geometry on the pool boiling heat transfer of FC-72 in high porosity aluminum metal foam heat sinks. Hysteresis and incipience excursion are almost absent when the foam is vertically positioned. High ppi samples deteriorate heat transfer performance in the vertical orientation. The low ppi sample shows the first decreased and then the increased heat transfer characteristics with reduction in foam heights. The temperature jump, marking transition from nucleate to film boiling, and the critical heat flux both increase with decreasing height in the low ppi sample for both orientations.

Moghaddam and Ohadi (2003) studied pool boiling heat transfer of water and FC-72 on thin blocks bonded with copper foams of 80 ppi, 90% porosity, 30 ppi, 95% porosity and graphite foam of 75% porosity. Significant enhancement was achieved in boiling of water on the 30 ppi copper foams, while no enhancement was observed on the 80 ppi copper and graphite foams. A substantial enhancement was achieved on all the foams with FC-72 as the working fluid.

Coursey et al. (2005) investigated the thermal performance of a graphite foam thermosyphon evaporator and discussed the foam's potential for use in the thermal management of electronics. Using the graphite foam as the evaporator in a thermosyphon enables the transfer of large amounts of heat, with low temperature difference and without the external pumping. The system performance with FC-72 and FC-87 was examined, and the effects of liquid fill level, condenser temperature, and foam height, width, and density were studied. Performance was found to be similar with FC-72 and FC-87. The liquid fill level, condenser temperature, geometry and density, of the graphite foam were found to influence the thermal performance significantly. The boiling was found to be surface tension dominated, and a simple model based on heat transfer from the outer surface is proposed. The maximum heat flux of 149 W/cm^2 was reached.

The above review on pool boiling heat transfer with enhanced micro-structures shows that the general agreement is not reached at this stage. The objective of this paper is to pursue the possibility that metal foams can be used for boiling heat transfer enhancement. We perform experiments over wide parameter ranges, not only for the

lower surface superheat applications, but also for the high surface superheats and heat fluxes. The objective of the paper is summarized as follows:

- Perform high speed visualizations of pool boiling heat transfer on copper foam covers, to identify boiling patterns.
- Perform thermal performance measurements of enhanced boiling heat transfer using copper foams, over very wide parameter ranges.
- Explain thermal performance of pool boiling heat transfer on copper foams by the observed boiling patterns.
- Identify the effects of ppi, thickness of foam cover, and pool liquid temperature on the thermal performance.

2. Copper foam and the characteristic parameters

Fig. 1 shows pictures of various copper foams, for the ppi of 30, 60 and 90, porosity of 0.88 and 0.95. The foam has an open-celled structure composed of dodecahedron-like cells, having 12–14 pentagonal or hexagonal faces. Two parameters characterizing foam cells are the ppi and porosity. The crosssection of ligaments depends on porosity, and changes from a circle at $\varepsilon = 0.85$ to an inner

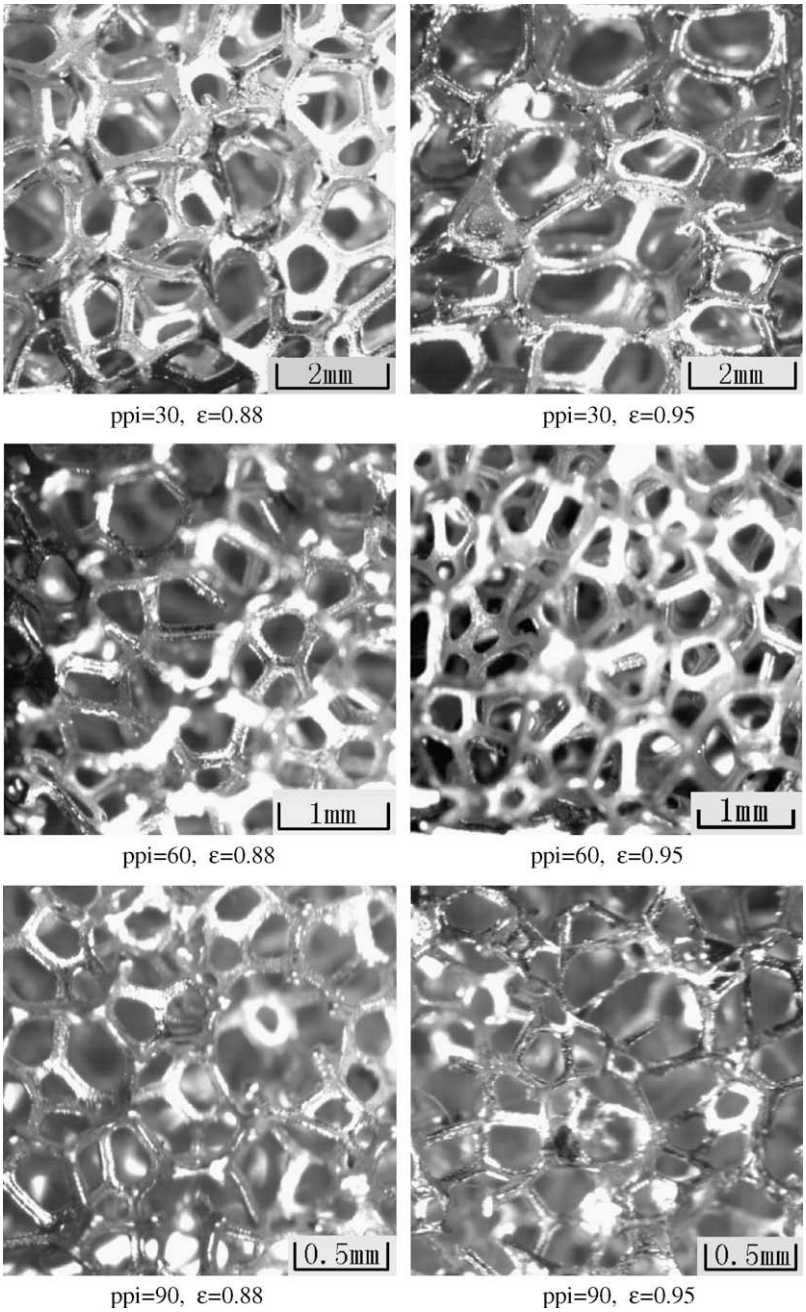

Fig. 1. Copper foam pictures.

concave at $\varepsilon = 0.97$ (Calmidi, 1998), where ε is the porosity. A unit cell of the foam is shown in Fig. 2, with the assumed tetrakaidecahedron shape. The ligament length is l with its diameter of d_f. Thus the volume of a unit cell is $V = 8\sqrt{2}l^3$. The circumcircle diameter of the foam cell is $\sqrt{10}l$, which can be regarded as the pore diameter of d_p, not considering the ligament thickness, i.e., $d_p = \sqrt{10}l$.

Table 1 shows the foam cell parameters measured by a Leica M-type microscope (Germany). It is seen that larger ppi yields smaller pore diameter of d_p and ligament diameter of d_f. When ppi is fixed, larger porosity such as 0.95 leads to slight larger d_p and smaller d_f, compared with the lower porosity of 0.88.

3. Experimental setup and procedures

3.1. The copper block welded with copper foam cover

The copper block was used to fabricate the test section. Fig. 3a shows geometry and size of the test section. In the bottom part of the copper block there are five 6.0-mm diameter holes, in which five cartridge heaters were inserted, providing heating power to the copper block. Each heater provides a maximum power of 100 W at the applied AC voltage of 220 V. In the middle part of the copper block, there are four 1.0-mm diameter holes, inside which four K-type thermocouples are inserted. The top of the copper block is a rectangular plate, having a thickness of 3.0 mm. A plain smooth, sand polished copper surface is regarded as the reference for boiling heat transfer experiments, with the size of 12.0 mm by 12.0 mm. Alternatively, the top copper surface was welded with copper foam

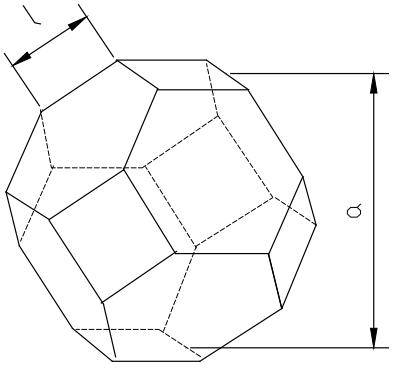

Fig. 2. A unit foam cell represented by a tetrakaidecahedron unit.

Table 1
Parameters of foam cells used in the present paper

Ppi	ε	d_p (mm)	d_f (mm)	l (mm)	d_f/d_p
30	0.88	2.762	0.314	1.074	0.114
30	0.95	3.285	0.286	1.181	0.087
60	0.88	1.192	0.141	0.486	0.118
60	0.95	1.491	0.124	0.541	0.083
90	0.88	0.696	0.081	0.275	0.116
90	0.95	0.772	0.064	0.299	0.083

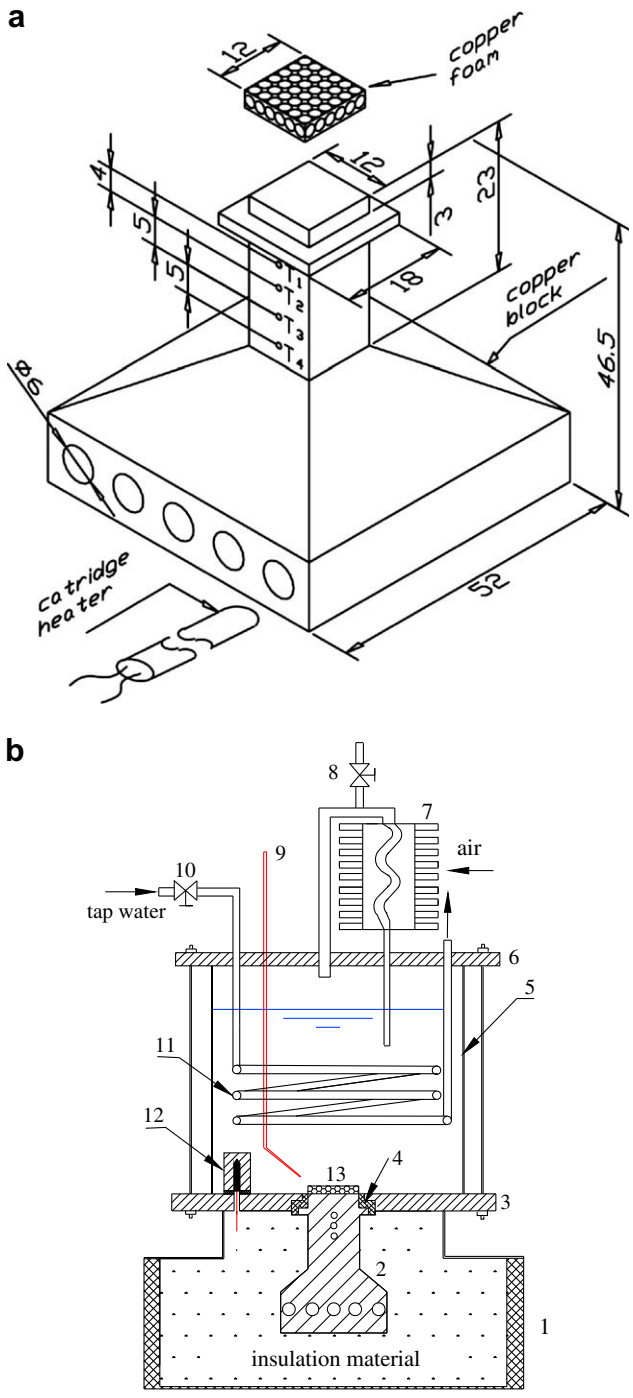

Fig. 3. Copper block test section and experimental setup. Note: all dimensions are in mm in (a).

covers, with the thickness of 2.0, 3.0, 4.0 and 5.0 mm, respectively. Once the copper block was ready, it was cleaned by methanol and baked in an oven. Then it was taken out of the oven and heated by the cartridge heaters until its temperature reached the melting temperature of the tin at the top copper surface, leaving a thin tin film. We put a clean foam cover on the copper surface and turned off the cartridge heaters, thus the copper foam was welded with the copper block tightly, which is ready

for experiments. The welding procedure ensures small thermal resistance between the copper block and the foam cover.

After the experiments, we removed the foam cover from the copper block when the copper block temperature approached the melting temperature of tin by heating the cartridge heaters. Then we sliced the foam cover in its thickness direction and visualized the separated piece of the foam cover by a microscope, showing that the tin thickness wicked into the foam cells is about 0.1 mm.

3.2. Experimental setup

Fig. 3b shows the experimental setup. A transparent glass chamber with the size of 125 × 127 × 145 mm was used to contain liquid. The bottom of the glass chamber was a stainless steel plate (3), at the center of which a rectangular hole was drilled. The copper block (2) was fitted with the plate (3) by filling Teflon and epoxy glue between them for seal, ensuring the copper foam exposed in the pool liquid. The part of the copper block under the plate (3) was surrounded by a glass sheath (1). As the thermal insulation material, glass fiber was filled in the gap between the copper block (2) and the glass sheath (1), as shown in Fig. 3b.

The top cover of the glass chamber was a stainless steel plate (6) with a 2.0 mm thickness. An inclined 6.0-mm diameter coiled copper tube (11) was arranged along the internal wall surface of the glass chamber. The two ports of the coiled tube penetrated the two holes of the plate (6). The copper tube outside of the glass chamber was connected with a tap water system. The pool liquid temperature could reach a desired value by adjusting the flow rate of tap water in the coiled tube (6) using the valve (10). An auxiliary heater (12) was installed in a corner of the glass chamber. During the boiling experiment, when the pool liquid temperature was below the desired value, the auxiliary heater (12) was turned on while the valve (10) was turned off. Such cases only occurred at very small heating power applied on the test section. However, most cases needed to maintain an adjustable flow rate of the tap water in the tube (11), with the auxiliary heater (12) turned off. The produced vapor during the boiling entered a reflux condenser (7). The condensed liquid returned to the glass chamber by gravity. Outside of the condenser was a fin heat sink cooled by forced convective air. The condenser was vented to atmosphere by the valve (8) through a side branch tube. Thus atmospheric pressure was always kept in the glass chamber. The pool liquid temperature was measured by a K-type thermocouple (9).

3.3. Measurement system and experimental procedures

Fig. 4 shows the measurement system. Five cartridge heaters were driven by a power supply system, consisting of a 220 V voltage stabilizer, a voltage transformer and a power meter. By adjusting the voltage transformer, one could obtain an adjustable voltage from 0 to 220 V, yielding a specific power supplied to the copper foam from 0 to 500 W. A precise power meter gave the power reading.

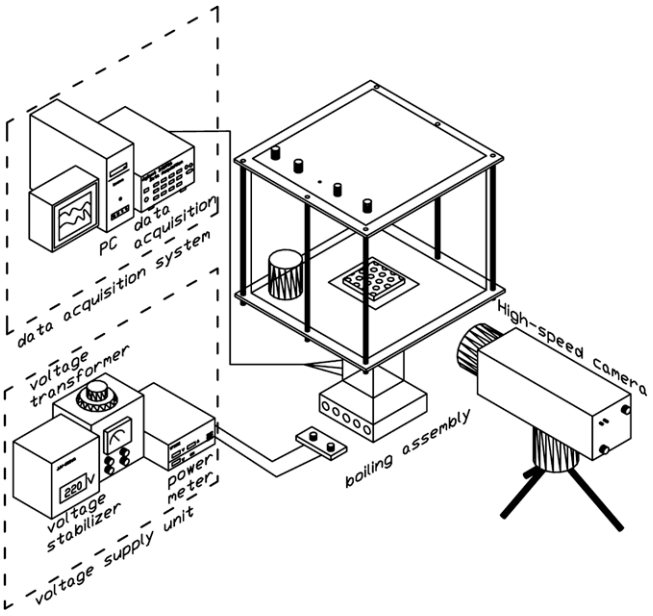

Fig. 4. Experimental setup and measurement system.

A Hewlett-Packard data acquisition system was used to collect the pool liquid temperature and four thermocouple signals (see Fig. 3a). A high speed camera system (HG-100K, Redlake Inc., USA) was used to capture the boiling patterns. The camera used the advanced 1.7 Megapixels CMOS sensor, which has a maximum recording rate of 20,000 images per second, with the sensitivity of 1504 × 1128 pixels. In order to clearly observe the boiling pattern in and out of foam cells, a micro-lens was adapted in front of the camera. In the present study, the recording rate of 5000 images per second was used.

The experimental procedure involved an initial charge of liquid in the glass tank and removing non-condensable gas. The copper foam cover was horizontally positioned. The top liquid level was higher than the top foam cover by 100 mm. Before the experiment, the cartridge heaters were turned on to vigorously boil the liquid for one hour to remove non-condensable gas in foam cells and liquid. The heaters were then turned off and the liquid was cooled to reach the environment temperature. The working fluid was acetone, with the thermo-physical properties given in Table 2 (Yaws, 1999). Most of previous studies used FC-72 as the working fluid. Acetone has the surface tension of 0.0192 N/m, comparable with FC-72 for the value of 0.00835 N/m, at room temperature. At atmospheric pressure, the latent heat of evaporation is 512.94 kJ/kg for acetone, significantly larger than the value of 94.80 kJ/kg for FC-72.

For each experiment, we started from a small heat flux 1–2 W/cm^2 on the copper foam and fixed the pool liquid temperature. If the variation of the copper block

Table 2
Physical properties of acetone at atmosphere pressure

T_{sat} (°C)	ρ_f (kg/m^3)	C_{pf} (J/kg K)	C_{pg} (J/kg K)	h_{fg} (kJ/kg)	σ (N/m)	μ_f (Pa s)	k_f (W/mK)
56.29	748.01	2302.5	1380.6	512.94	0.0192	0.000237	0.518

Where T_{sat} is the saturated temperature, ρ_f is the liquid density, C_{pf} and C_{pg} are the specific heat of liquid and vapor, h_{fg} is the latent heat of evaporation, σ is the surface tension, μ_f is the liquid viscosity, k_f is the thermal conductivity of liquid.

temperature was smaller than 1 °C in 10 min, the heat transfer process was considered to reach a steady state. After that, we recorded the pool liquid temperature, the four temperatures on the copper block and the power meter reading. We recorded transient boiling patterns by the high speed camera, noting that not all the cases were recorded by the camera.

We then increased the heat flux by a small step of 2–5 W/cm^2, and repeated the above procedure. Attention was paid at boiling incipience, around which a very small increment of heat flux ~1 W/cm^2 was used. Same procedure was performed for all the experiments in this paper.

The heat flux was computed as $q = -k\frac{dT}{dz}|_{\text{base surface}}$ based on the one-dimensional heat conduction equation, where k is the copper thermal conductivity, $\frac{dT}{dz}|_{\text{base surface}}$ is the temperature gradient at the base surface, z is the coordinate perpendicular to the base surface. A least square correlation of temperatures versus z was written as $T = a_0 + a_1 z$, where a_0 and a_1 are constants correlated based on T_1, T_2, T_3 and T_4 (see Fig. 3a). The heat flux uncertainty was estimated to be smaller than 6.0%. The surface superheat ΔT_{sat} is defined as the surface temperature of T_w minus T_{sat}, where T_w is the temperature at the base surface, T_{sat} is the saturated temperature of acetone at atmospheric pressure. The heat transfer coefficient is calculated as

$$h = q/(T_w - T_{bulk}) \tag{1}$$

where T_{bulk} is the pool liquid temperature. The surface temperature, surface superheat and pool liquid temperature have the maximum uncertainties of 0.3 °C.

Now we estimate uncertainty of the heat transfer coefficient, which is a function of three independent variables of q, T_w and T_{bulk}. The uncertainty of h is computed as

$$\Delta h = \sqrt{\left(\frac{\partial h}{\partial q}\right)^2 \Delta q^2 + \left(\frac{\partial h}{\partial T_w}\right)^2 \Delta T_w^2 + \left(\frac{\partial h}{\partial T_{bulk}}\right)^2 \Delta T_{bulk}^2} \tag{2}$$

Thus the relative uncertainty can be calculated by substituting Eq. (1) into Eq. (2) as

$$\frac{\Delta h}{h} = \sqrt{\left(\frac{\Delta q}{q}\right)^2 + \left(\frac{\Delta T_w}{T_w - T_{bulk}}\right)^2 + \left(\frac{\Delta T_{bulk}}{T_w - T_{bulk}}\right)^2} \tag{3}$$

In Eqs. (2) and (3), Δq, ΔT_w and ΔT_{bulk} are the uncertainties of heat flux, wall surface temperature and pool liquid temperature. The maximum uncertainty of h is obtained by a smaller surface temperature and a larger pool liquid temperature. Thus we acquire the maximum relative uncertainty of h as 8.52%.

We estimate the non-condensable gas concentration in acetone. In terms of Kretschmer et al. (1946), the mole fraction of dissolved air in acetone is about 6×10^{-4} at room temperature of 25 °C and atmospheric pressure of 101.3 kPa. The saturated vapor pressure of acetone is expressed as (Yaws, 1999)

$$\log_{10}\left(\frac{p_v}{760} \times 1.013 \times 10^5\right) = 28.588 - \frac{2469}{T_{bulk}} - 7.351 \times \log_{10} T_{bulk} + 2.736 \times 10^{-6} \times T_{bulk}^2 \tag{4}$$

where p_v and T_{bulk} have the units of Pascal and Kelvin.

The values of p_v are 30.6, 52.1 and 75.9 kPa at the three temperatures of 25, 38 and 48 °C, respectively. It is difficult to measure the non-condensable gas concentration, but we calculate the gas concentration in acetone based on the Henry's law: $S_{gas} = k_H p_{gas}$, where S_{gas} is the gas solubility, k_H is the Henry's constant, p_{gas} is the gas pressure which is $p_{gas} = p - p_v$, p is the pressure in the glass chamber of this study. Our estimation gives the mole fraction of air in acetone is 4.2×10^{-4} and 2.2×10^{-4} at the liquid temperatures of 38 and 48 °C, respectively, showing the decreased non-condensable gas concentration with increasing temperatures.

This study covers the following data ranges: ppi of 30, 60, 90; porosity of 0.88 and 0.95; foam cover thickness of 2.0, 3.0, 4.0 and 5.0 mm; surface superheat from −20 to 190 K; surface heat flux up to 140 W/cm^2. It is noted that the heat flux is based on the top copper surface area of 12.0 mm by 12.0 mm. The foam cell area is not involved in the computation of heat flux.

4. Results and discussion

4.1. Visualization of boiling patterns

4.1.1. Visualization for the 30 ppi foam covers

High speed visualizations were performed. Fig. 5a shows the boiling pattern near the boiling incipience at $q = 8.3$ W/cm^2 and $\Delta T_{sat} \approx 4$ K. The copper foam has the ppi of 30 and porosity of 0.88 with the thickness of 3.0 mm. Miniature bubbles nucleate at the foam ligaments and fiber junctions in foam cells. Initial nucleation sites mostly take place at specific locations. The nucleated bubble evolves a growth and departure process, finally is released to the pool liquid. Fig. 5b shows the miniature bubble nucleation, growth and release to the pool liquid at $q = 10.4$ W/cm^2. Active nucleation sites are increased compared with those shown in Fig. 5a. The steady state boiling heat transfer is well maintained with foam cells immersed in liquid.

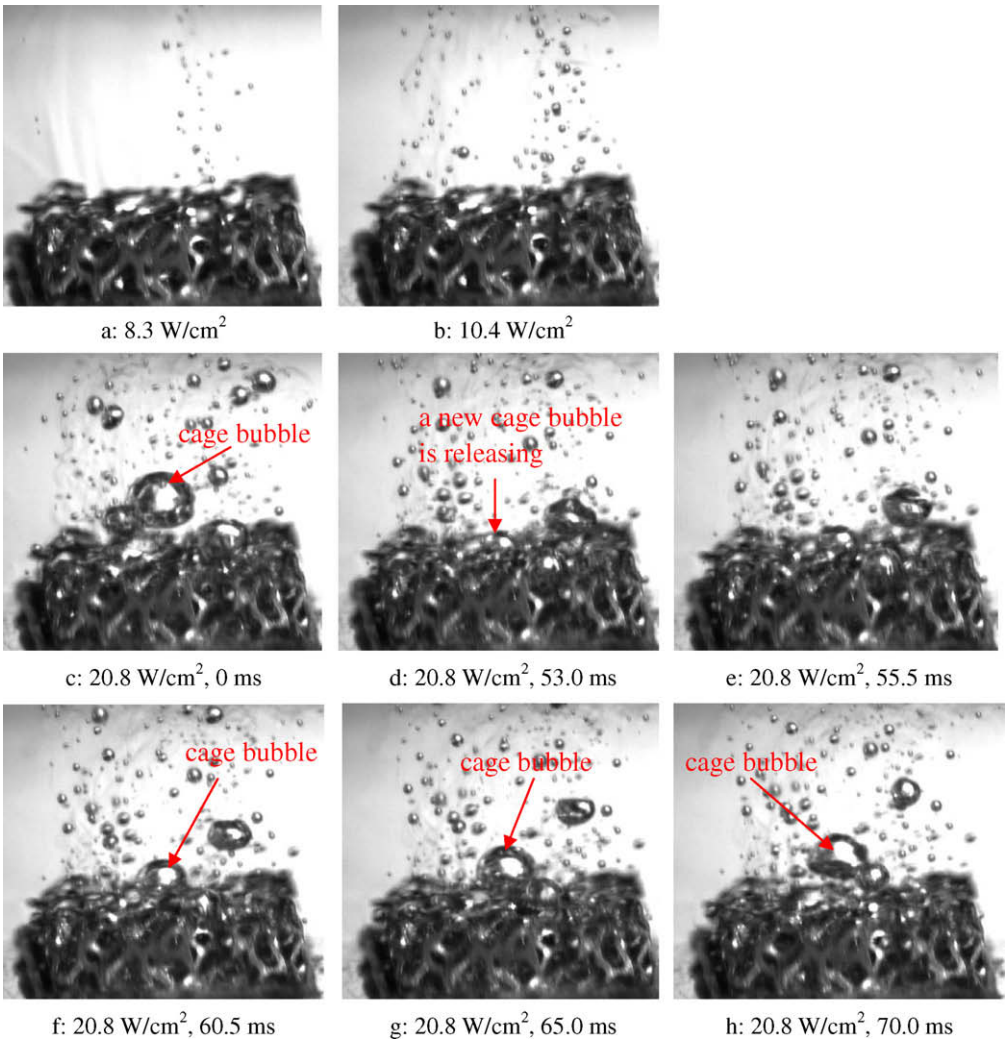

Fig. 5. Boiling pattern at boiling incipience and low heat flux (ppi = 30, $\varepsilon = 0.88$, $T_{bulk} = 38$ °C, $\delta = 3.0$ mm, ΔT_{sat} equals to 3.7 K for (a), 4.1 K for (b) and 8.0 K for (c–h)).

A small increase in surface superheat greatly raises the heat flux. Photographs in Fig. 5a and b show the periodic single bubble generation and departure pattern without coalescence.

Increases in heat fluxes lead to bubble coalescence before release to the pool liquid, as shown in Fig. 5c–h at $q = 20.8$ W/cm^2. A new cycle begins at the time when a cage bubble is fully separated from the foam cells and enters the pool liquid (Fig. 5c). Cage bubble comes from the coalescence of miniature bubbles in foam cells. Then the boiling heat transfer is sustained with nucleation and growth of miniature bubbles in foam cells for a longer time such as 55.5 ms, which can be considered as the waiting time for bubble coalescence. A new cage bubble appears and gradually penetrates the foam cover for $t > 55.5$ ms (Fig. 5d–g), until it is out of the foam cover and the present cycle ends at $t = 70.0$ ms (Fig. 5h). Thus the cycle period is about 70 ms and the formation/release frequency of the merged bubble is 14.3 Hz. Because the heat flux is not sufficiently high, coalescence of miniature bubbles takes place at the specific area, such as the foam cover center. In contrast to Fig. 5a and b, Fig. 5c–h shows the periodic bubble coalescence pattern, noting that cage bubble appears in Fig. 5c–h and it will also be shown in the following figures, the cage bubble formation will be given in Section 4.1.2.

Further increase in heat fluxes yields spreading of merged bubbles over the whole foam cover. Fig. 6 shows the periodic bubble coalescence and re-coalescence pattern at $q = 83.3$ W/cm^2. A similar cycle definition is used. A mushroom-shaped cage bubble is fully separated from the foam cover, defined as the beginning of a new cycle shown in Fig. 6a. Miniature bubbles generated in foam cells are quickly merged to form a set of cage bubbles, covering the whole foam cover (Fig. 6b and c). The waiting time for bubble coalescence is greatly shortened and not apparent. This is the first stage for bubble coalescence. Bubble re-coalescence begins at $t = 19.0$ ms (Fig. 6c). There are six merged bubbles at that time. Then these bubbles are re-merged to have two cage bubbles (Fig. 6d and e). Finally a single big mushroom-shaped cage bubble is released to

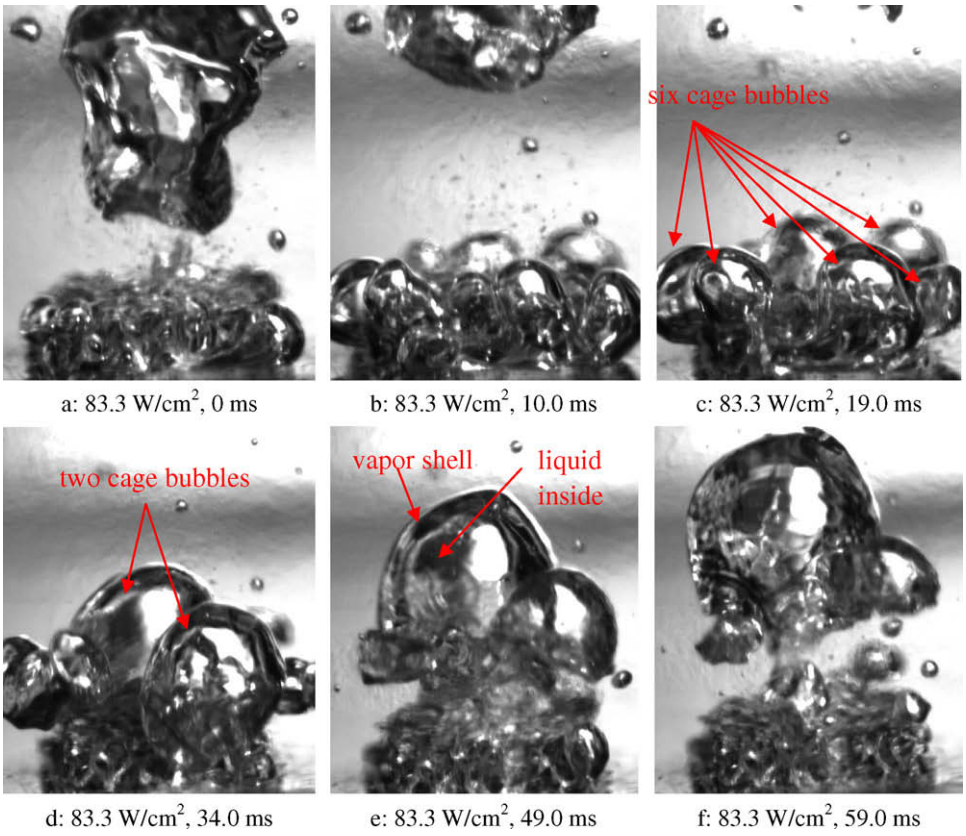

Fig. 6. Boiling pattern at $q = 83.3$ W/cm^2 (ppi = 30, $\varepsilon = 0.88$, $T_{bulk} = 38$ °C, $\delta = 3.0$ mm).

the pool liquid at $t = 59.0$ ms (Fig. 6f), ending the present cycle. Again cage bubbles have "open" centers filled with liquid. Fig. 6 shows the periodic bubble coalescence and re-coalescence pattern.

A similar boiling pattern is shown in Fig. 7 at $q = 112.0$ W/cm^2 just before CHF. Boiling heat transfer is so violent that bubble coalescence evolves very quickly to form a very big mushroom-shaped cage bubble (Fig. 7d and e). The cage bubble can surround the whole foam cover, including the four sides of the foam cover. As the time during which the whole foam cover is occupied by the vapor phase consists of a larger percentage of a full cycle period, liquid suction towards the foam cells becomes difficult. A small increase in heat flux such as 1 W/cm^2 leads to an uncontrollable temperature rise of the copper block, reaching the CHF condition.

4.1.2. Cage bubble formation

Enhanced boiling heat transfer has been extensively studied for several decades. However, cage bubbles are not reported previously. Again, Fig. 8a and b shows the enlarged cage bubble structure for the same run case of Fig. 6. There are two cage bubbles shown, marked as the front one and the behind one. Both of them have a vapor shell and a liquid center vented to the pool liquid. The direction of the liquid center is perpendicular to the paper plane. The front bubble is "open" so that the vapor shell of the behind one can be completely visualized. Fig. 8c shows a typical encircled cage bubble structure at the heat flux same as that of Fig. 7. Two cage bubbles are shown with the smaller one inside the bigger one. The bigger bubble is "open" so that the smaller one can be seen. Fig. 8 provides the direct experimental evidence of the cage bubbles.

A rough explanation of the cage bubble is given here. When miniature bubbles merge to a big bubble, the big bubble has the size larger than a unit foam cell. A foam ligament changes its direction when it crosses the ligament junction. The arranged foam ligaments stab the big bubble, or we can say that the big bubble is plunged by the continuous ligaments. When the big bubble is departing from the stationary foam cells, the space that was previously occupied by the foam ligaments and junctions inside the bubble should be further replaced by liquid. The newly formed liquid volume is from the integrated flow rate of the liquid film around the foam ligament surfaces. The liquid flow rate is sucked from the pool liquid to the inner bubble. When the big bubble is fully detached from foam cells, the space that was previously occupied by the foam ligaments and junctions before bubble departure becomes liquid filled and vented to the pool liquid. Surface tension force smoothes vapor–liquid interface inside the bubble, forming a single liquid filled center. Cage bubble is formed due to the connected web structure of foam ligaments through junctions. The cage bubble formation needs further investigation.

Wei and Honda (2003) visualized boiling patterns of FC-72 from silicon chips with micro-pin-fins immersed in

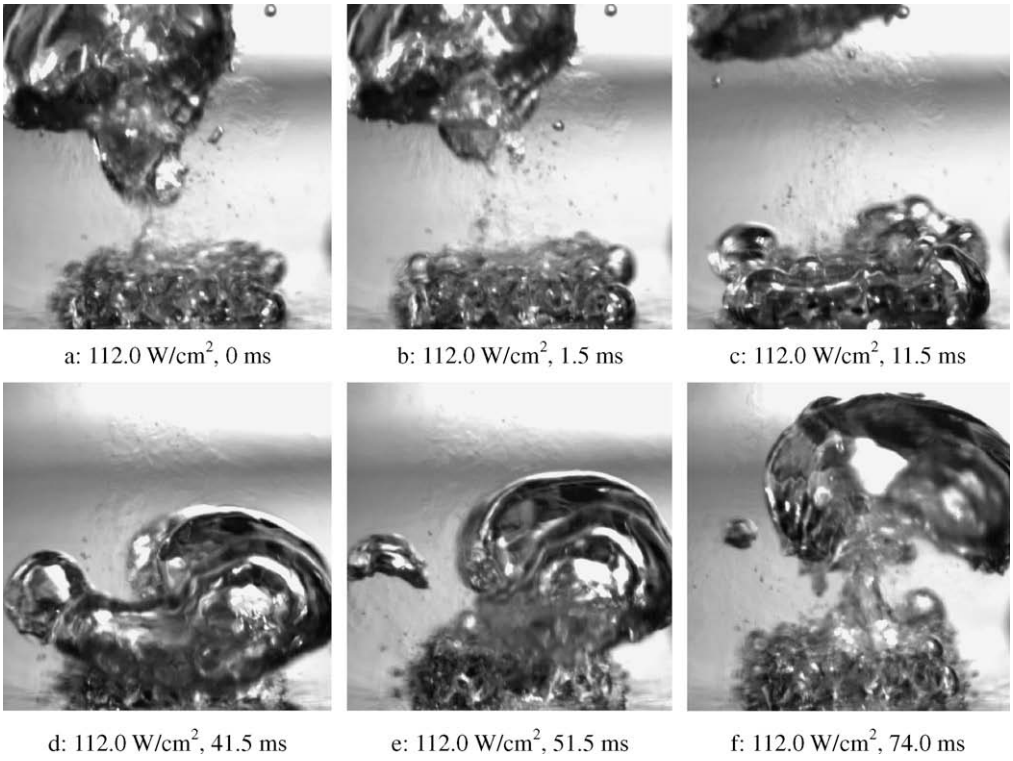

Fig. 7. Boiling pattern at $q = 112.0$ W/cm^2 (ppi = 30, $\varepsilon = 0.88$, $T_{bulk} = 38$ °C, $\delta = 3.0$ mm).

FC-72. Single miniature bubble at low heat fluxes and bigger merged bubble at high heat fluxes were reported. Parker and El-Genk (2005) presented photographs of nucleate boiling of FC-72 on the porous graphite. They showed the higher density of detaching bubbles from the porous graphite surface, which is consistent with the measured enhancements in nucleate boiling heat transfer coefficients. Other visualizations of bubble dynamics during pool boiling on enhanced structures were given by Chen et al. (2005), Ghiu and Joshi (2005), Nimkar et al. (2006), Meléndez and Reyes (2006). Cage bubble is not reported in these references.

4.1.3. Visualization for the 90 ppi foam covers

The observed boiling patterns on the 60 ppi foam covers are similar to those on the 30 ppi ones. Now we show boiling patterns on the 90 ppi foam covers. The larger the value of ppi, the smaller the pore diameter of d_p is. As shown in Table 1, d_p is 2.76 mm for the 30 ppi foam at $\varepsilon = 0.88$. But d_p is decreased to 0.70 mm for the 90 ppi foam at the same porosity. The small pore size for large ppi foams leads to easy coalescence of miniature bubbles at low heat fluxes, see Fig. 9a and b at $q = 5.8$ and 6.9 W/cm^2, respectively. A single merged cage bubble is generated and detached periodically. Fig. 9c–f shows the boiling pattern for a full cycle at $q = 12.5$ W/cm^2. Two merged cage bubbles instead of one are being generated and departing from the foam cover synchronously.

The periodic bubble coalescence pattern does not exist at moderate or high heat fluxes for the high ppi foams. Fig. 10 shows boiling patterns at the heat fluxes of 41.0, 62.5 and 118.1 W/cm^2. Boiling process is violent without cycle behavior demonstrated. Vapor fragments are continuously departing to the pool liquid. Liquid is sucked towards the foam cover through miniature gaps between neighboring fragments (counter-current vapor–liquid flow). Small pore size of large ppi foam cells ensures strong pumping effect for liquid suction towards the foam cells, which is helpful to maintain liquid film around the foam ligaments and junctions at moderate or high heat fluxes.

4.2. Boiling heat transfer of acetone on the foam covers

Boiling curves are shown in Fig. 11. The value of ppi is 30, 60 and 90 at $\varepsilon = 0.88$ and $\delta = 3.0$ mm, where δ is the foam cover thickness. Three pool liquid temperatures of 38, 48 and 55 °C were used. The pool liquid temperature of 55 °C approaches the saturated temperature of acetone at atmospheric pressure. The surface superheats vary over a wide range from −20 to 190 K, which is helpful not only for electronic cooling applications, but also for other applications with much high heat flux that require large surface temperature. Boiling curves on the plain smooth surface are shown for comparisons.

Fig. 11 demonstrates that copper foams not only enhance boiling heat transfer, but also significantly extend the operation range of surface superheats. The measured CHFs are 56.6, 40.4 and 37.2 W/cm^2 on the plain surface at the three pool liquid temperatures. Correspondingly, they are 114.3, 107.2 and 98.7 W/cm^2 on the 30 ppi foam

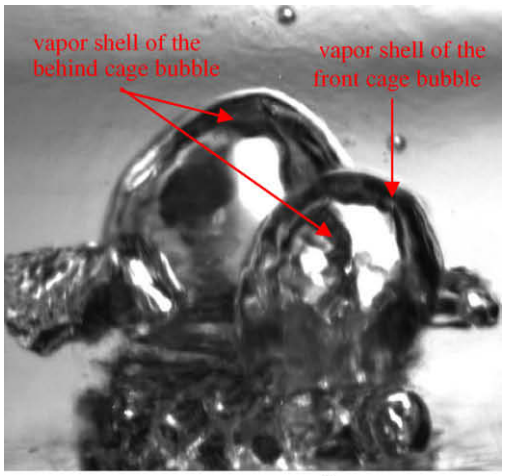

(a) 83.3 W/cm^2

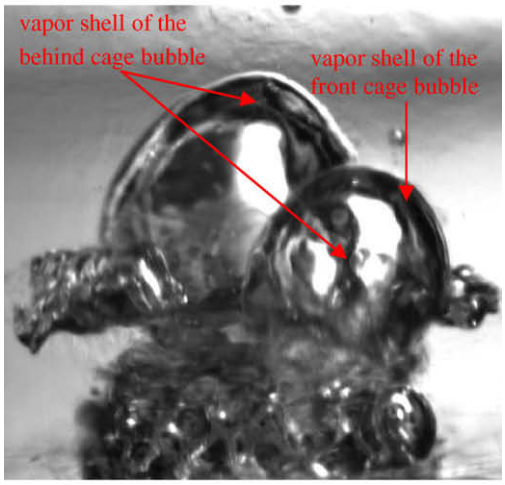

(b) 83.3 W/cm^2

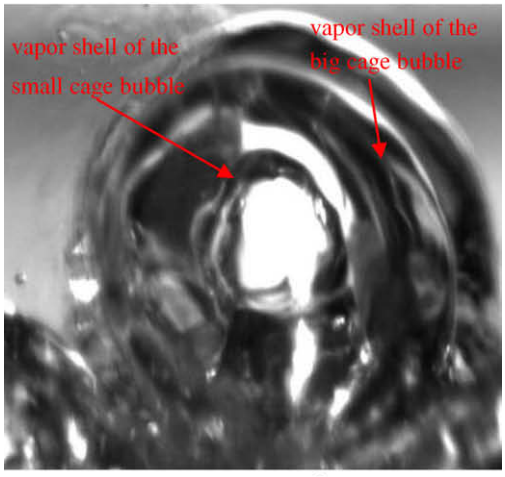

(c) 112.0 W/cm^2

Fig. 8. Cage bubble observed in the present study ((b) is elapsed with 3.0 ms following (a)).

covers. CHF is not reached at high surface superheats of 180–190 K on the 60 and 90 ppi foam covers. The measured CHFs are several times larger than those reported in references using FC-72 as the working fluid, such as Rainey and You (2000), Liter and Kaviany (2001), Kim et al. (2002), Honda and Wei (2004). This is mainly due to that acetone has larger latent heat of evaporation. CHFs are not previously reported for pool boiling heat transfer on the metallic foam covers. The range of surface superheats in this paper is usually quite larger than that in references.

Boiling curves of the foam cells can be divided into three distinct regions, which are marked as region I for liquid natural convection heat transfer, region II for nucleate boiling heat transfer, for all the foam cells. Region III is that of either the resistance to vapor release, for the 30 and 60 ppi foam covers, or the capillary-assist liquid flow towards foam cells for the 90 ppi foam covers. The different terms used for the third region for low and high ppi foam covers are due to the different boiling patterns observed, i.e., the periodic bubble coalescence and/or re-coalescence pattern for the 30 and 60 ppi foam covers, and the violent vapor fragments release pattern for the 90 ppi foam covers.

Slopes of boiling curves are significantly changed from region I to II, and from region II to III, corresponding to two transition points. Boiling incipience is the first transition point, at which the surface superheats are about 4 K on the three ppi foam covers at the pool liquid temperature of 38 °C (see Fig. 11a). Temperature excursions are not observed for all the foam covers in this study, which is qualitatively consistent with other studies such as Arbelaez et al. (2000) on the aluminum foams, Moghaddam and Ohadi (2003) on the copper and graphite foams. For comparison, the surface superheat is about 21 K on the plain smooth surface at boiling incipience. The second transition point from region II to III occurs at the surface superheats of 20 and 24 K on the 30 and 60 ppi foam covers, respectively. Heat fluxes at the second transition point strongly depend on the value of ppi. Higher ppi foams greatly decrease heat fluxes at the second transition point, indicating the increased resistance to vapor release for the high ppi foam covers. It is known from Fig. 11 that higher pool liquid temperatures slightly decrease slopes of boiling curves in region II. Generally the three subfigures in Fig. 11 show similar trend at different pool liquid temperatures.

In a general sense, enhancement of pool boiling heat transfer on foam covers is attributed to the combined effect of an extended surface area, an increased nucleation site density, the resistance to vapor release from foam cells, and a capillary-assist liquid flow towards foam cells. The liquid supply and vapor release occur as a liquid–vapor counterflow resisting each others motion. Meléndez and Reyes (2006) gave a correlation to compute the vapor flow rate escaping from the porous coverings:

$$m = \frac{\pi}{128}\left(\frac{\rho_v \sigma}{\mu_v}\right)\left(\frac{\varepsilon d_p^3}{\delta}\right) \tag{5}$$

where ρ_v and μ_v are the vapor density and viscosity, respectively. Eq. (5) indicates the influence of the thermophysical properties (ρ_v, σ, μ_v) and the porous parameters

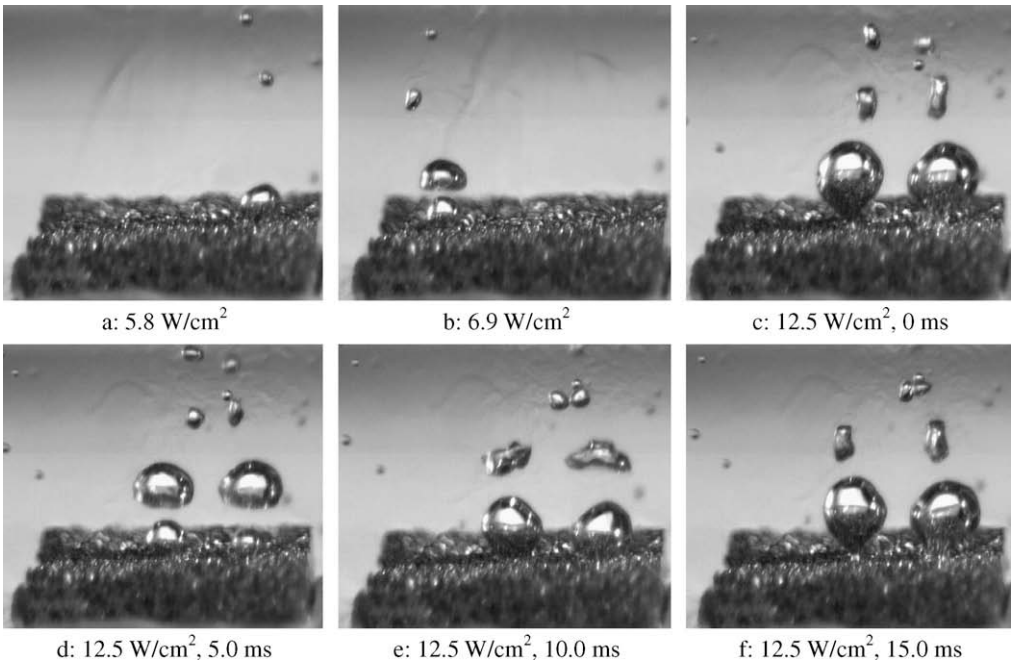

Fig. 9. Boiling pattern at low heat fluxes (ppi = 90, $\varepsilon = 0.88$, $T_{bulk} = 38$ °C, $\delta = 3.0$ mm).

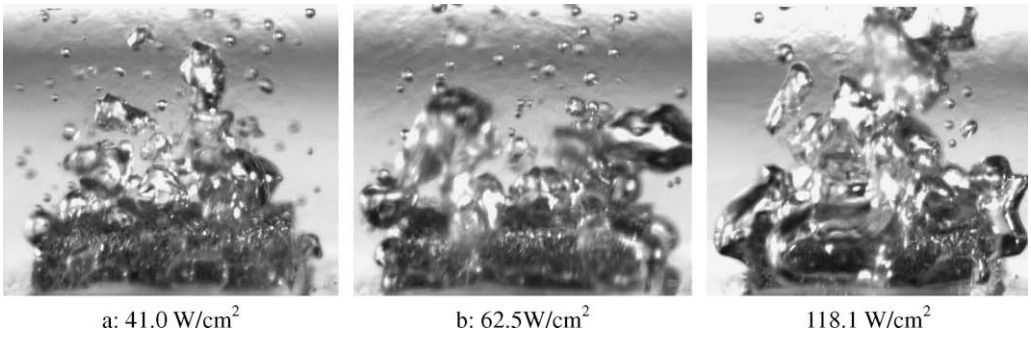

Fig. 10. Boiling pattern at moderate and higher heat fluxes (ppi = 90, $\varepsilon = 0.88$, $T_{bulk} = 38$ °C, $\delta = 3.0$ mm).

$(\varepsilon, d_p, \delta)$. A larger vapor mass flow rate represents a smaller resistance to vapor release. At the same porosity ε, low ppi foam covers have large pore size of d_p, leading to a large value of m. On the other hand, the capillary pressure pumping liquid flow towards foam cells is related to $2\sigma/d_p$. Thus it is seen that small pore size of high ppi foam covers retards vapor escaping from foam cells, but has large capability for pumping liquid to the phase change surface.

In the nucleate boiling region (region II), the surface superheats are not large, showing the periodic single bubble generation and departure pattern (Fig. 5a and b), or the periodic bubble coalescence pattern (Fig. 5c–h). The extended surface area of foam cells and increased nucleation sites significantly enhance heat transfer. The generated vapor is freely released while the liquid suction towards the phase change surfaces is sufficient. A large increase in heat flux only yields a small increase in surface superheat, maintaining good thermal performance. Fig. 11 shows that low ppi foams have slightly better heat transfer performance in region II.

In region III, the 30 and 60 ppi foam covers show the periodic bubble coalescence and re-coalescence pattern such as given in Figs. 6 and 7, contrast to the continuous vapor fragment release pattern given in Fig. 10 for the 90 ppi foam covers. This difference directly leads to different heat transfer performances on low and high ppi foam covers. The resistance to vapor release is important, while the liquid pumping effect is weak, on the 30 and 60 ppi foam covers. The 30 ppi foam covers (largest pore diameter of d_p) provides less resistance to vapor release, leading to better heat transfer performance than the 60 ppi foam covers. As shown in Fig. 11, the 30 ppi foam covers increase heat fluxes by 20–25 W/cm^2 than the 60 ppi foam covers at the same surface superheat, in region III.

The capillary-assist liquid pumping effect is important for the 90 ppi foam covers in region III. At sufficiently high heat fluxes $\sim$100 W/cm^2, the 90 ppi foam covers with smallest pose size has strong capability to suck liquid towards the phase change surfaces, preventing fully dry-out in foam cells and thus delaying appearance of CHF.

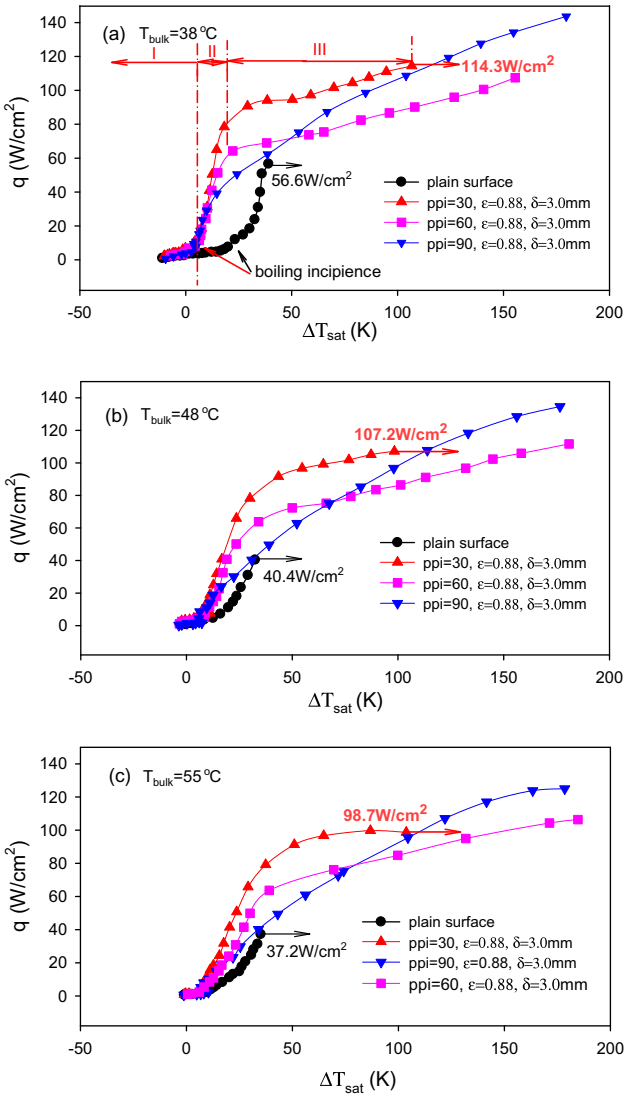

Fig. 11. Boiling curves for three ppi foams at three pool liquid temperatures.

The largest heat flux is always reached on the 90 ppi foam covers in this study. Meanwhile, the strong liquid pumping effect for the 90 ppi foam covers leads to steeper slope of boiling curves than the 30 and 60 ppi foam covers, causing the crossover of boiling curves between the 90 and 60 ppi foam covers (see Fig. 11). The crossover of boiling curves between the 90 and 30 ppi foam covers are not apparent because the 30 ppi foam covers have smaller range of surface superheats. In region III, the difference of slopes of boiling curves between the 30 and 60 ppi foam covers is not large.

4.3. Parameter effects on boiling heat transfer of foam cells

Larger porosity such as $\varepsilon = 0.95$ provides less space occupied by the solid material and decreases the surface area of ligaments and junctions. Fig. 12 shows boiling curves at $\varepsilon = 0.95$. Again, three heat transfer regions are

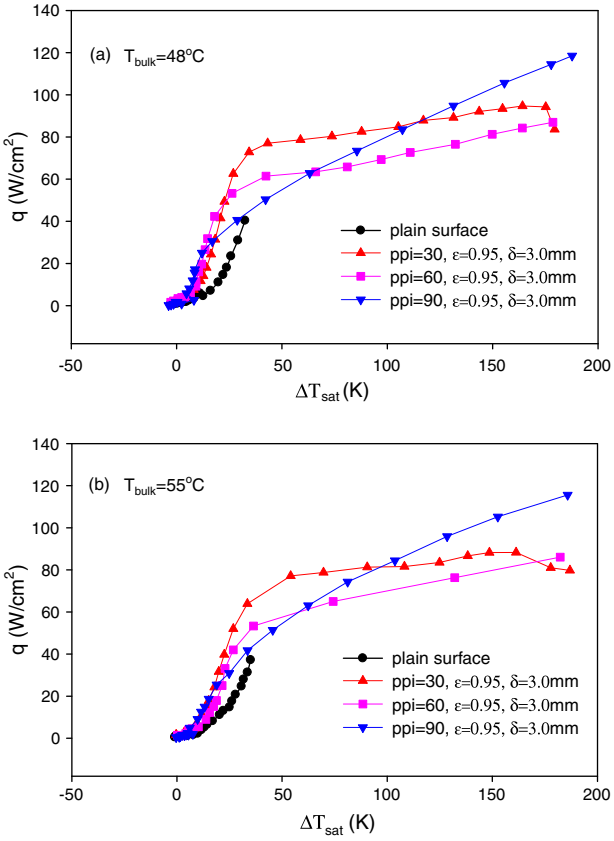

Fig. 12. Boiling curves for the foam porosity of 0.95.

identified. Compared with Fig. 11 at $\varepsilon = 0.88$, the range of surface superheats in natural convection heat transfer region becomes narrow for all the foam covers. But the entire range of surface superheats for the 30 ppi foam covers is extended. Boiling curves are crossed not only between the 90 and 60 ppi foam covers, but also between the 90 and 30 ppi foam covers.

Figs. 13 and 14 shows the effects of foam ppi, thickness of foam covers, and pool liquid temperature on heat transfer coefficients. Most curves show the increased, maximum and then decreased heat transfer coefficient with continuous increases in heat fluxes, i.e., the quasi-parabola distribution. The maximum heat transfer coefficient exactly takes place at the transition point from region II to III (see Fig. 11).

Fig. 13a shows the effect of ppi on heat transfer performance. Heat fluxes at the maximum heat transfer coefficients are significantly decreased with increasing ppi. For instance, the heat flux is 78 W/cm^2 for the 30 ppi foam cover, but it is 24 W/cm^2 for the 90 ppi foam cover, instead. Low ppi value delays the transition from region II to III. Heat transfer shows nucleate boiling mechanism before the maximum heat transfer coefficient, for all the ppi foam covers. Heat transfer coefficients are decreased beyond the maximum point for the 30 and 60 ppi foams due to the increased resistance to vapor release. They are almost independent of heat fluxes beyond the maximum

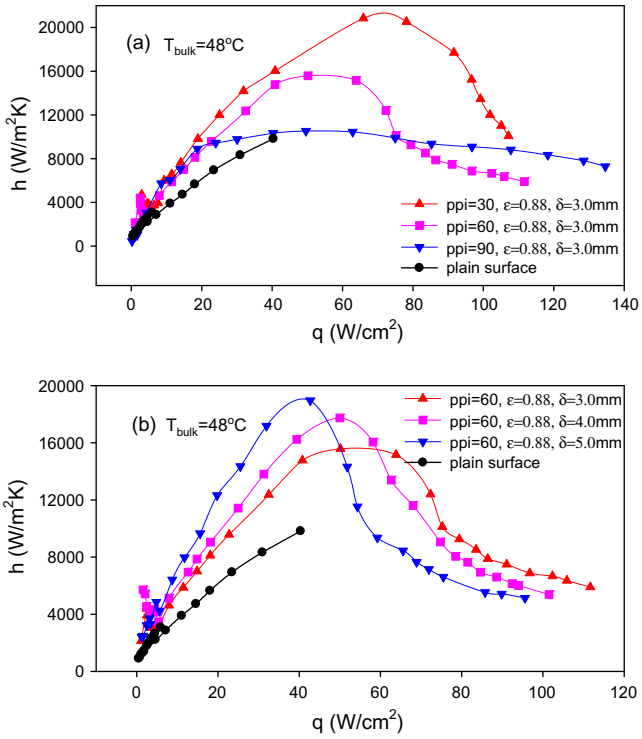

Fig. 13. Effect of ppi and foam cover thickness on heat transfer coefficients.

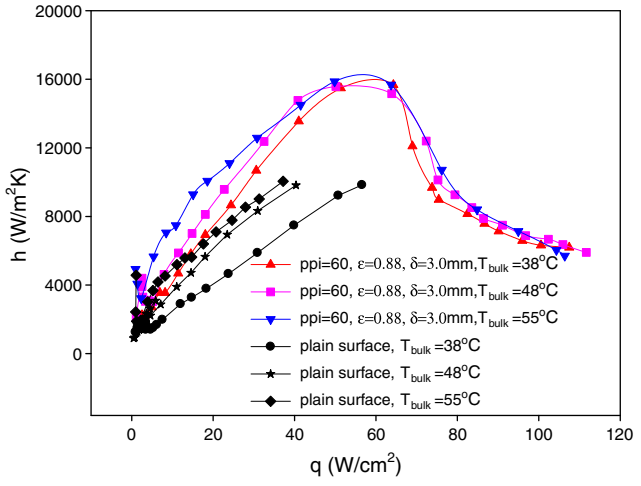

Fig. 14. Effect of pool liquid temperatures on heat transfer coefficients.

point for the 90 ppi foam covers in region III, which is thoroughly different from those for the 30 and 60 ppi foam covers (Fig. 13a).

Fig. 13b shows the effect of foam cover thickness on heat transfer coefficients. In region II (nucleate boiling region), an increase in foam cover thickness increases the bubble nucleation site density, enhancing heat transfer, under which the resistance to vapor release is not large and the liquid supply towards foam cells is sufficient. This is not true in region III. Large foam cover thickness increases the resistance to vapor release, lowering the heat transfer coefficients. It is noted that liquid suction can take place from both the four sides and the top surface of the foam cover. At moderate or high heat fluxes in region III, the generated vapor along the four internal margins of the foam cover prevents the success liquid suction from there. Thus liquid suction from the top surface of the foam cover is necessary to maintain the heat transfer process.

Fig. 14 shows the effect of pool liquid temperatures on heat transfer coefficients. Higher pool liquid temperature enhances nucleate boiling heat transfer in region II, before the maximum heat transfer coefficient. This is due to that higher pool liquid temperature activates more nucleation sites. However, in region III, pool liquid temperatures have small effect on the heat transfer coefficients. In such a region, heat transfer is mainly governed by the resistance to vapor release. The pool liquid temperature only has slight influence on the thermo-physical properties of the liquid phase.

Correlations for the heat transfer coefficients are difficult at this stage, due to the different heat transfer mechanisms in the three regions. Besides, the heat transfer mechanisms are different between the 90 ppi and low ppi foam covers in region III. Theoretical/numerical works are recommended to study the complex pool boiling heat transfer in metal foams.

4.4. Comparison with other studies

We performed high speed visualizations of pool boiling on the foam covers. The periodic single bubble generation and departure pattern at low surface superheats, and the periodic bubble coalescence and/or re-coalescence pattern at moderate or high surface superheats were observed on the 30 and 60 ppi foam covers. The 90 ppi foam cover makes the bubble coalescence at sufficiently low surface superheats, while it behaves the continuous vapor fragment release pattern at moderate and high surface superheats. For the above observations, cage bubble is a new phenomenon, as described in Section 4.1.2. Cage bubbles are formed due to the distinct connected web structure of foam cells.

We found that copper foams with open cells could decrease the surface superheat and eliminate the temperature excursion at boiling incipience, which is consistent with that drawn by other studies such as Wei and Honda (2003) for micro-pin-fin structure, Parker and El-Genk (2005) for graphite foams. Alternatively, Rainey and You (2000) noted that pool boiling heat transfer from microporous, square pin-finned surfaces decreases the surface superheat and temperature excursion at boiling incipience. But the temperature excursion is not fully eliminated for some run cases.

In this paper, we used acetone as the working fluid, having larger latent heat of evaporation than FC-72. Thus both the heat transfer coefficients and critical heat fluxes are much higher than those reported in references such as Rainey and You (2000), Liter and Kaviany (2001), Kim et al. (2002), Honda and Wei (2004). The degree that the

present data deviate from other studies depends on the heating surface area, the parameters of enhanced microstructure used.

We identified three heat transfer regions of pool boiling on copper foam covers. Region I and II refer to the liquid natural convection heat transfer and nucleate boiling heat transfer for all the foam covers. Region III is that of either the resistance to vapor release for the 30 and 60 ppi foam covers, or the capillary-assist liquid flow towards foam cells for the 90 ppi foam covers. Slopes of boiling curves are different in the three regions. Boiling curves are crossed between the 90 ppi and low ppi foam covers.

Parker and El-Genk (2005) studied pool boiling heat transfer of FC-72 on the porous graphite. Boiling curves are divided into the natural convection region and nucleate boiling region. Three sub-regions are divided for the nucleate boiling. Region I is that of low-superheat nucleate boiling. In region II, the slope of boiling curves is higher than that in region I. Bubble coalescence in region III reduces the slope of boiling curves with increased surface superheats. Thus the three heat transfer regions defined in this paper are different from those defined by Parker and El-Genk (2005). Arbelaez et al. (2000) investigated pool boiling heat transfer of saturated FC-72 in highly porous aluminum foams. The experiments covered porosities and ppi in the range of 90–98% and 5–40 ppi. The value of ppi that they used is significantly lower than that tested in the present paper. They found the increased heat transfer coefficients and critical heat fluxes compared with the plain surface. It is also noted that there is a transition from nucleate boiling to film boiling, accompanying a temperature jump at the transition point. This behavior is not observed in the present paper. However, the crossover of boiling curves identified in the present paper is not reported previously.

5. Conclusions

The conclusions drawn in this paper are summarized as follows:

1. The 30 and 60 ppi foam covers display the periodic single bubble generation and departure pattern at low surface superheats. They behave the periodic bubble coalescence and/or re-coalescence pattern with continuous increases in surface superheats. Cage bubble is a new phenomenon identified in the present paper.
2. The 90 ppi foam covers induce easy coalescence of miniature bubbles at small surface superheats, with the periodic bubble coalescence pattern demonstrated. At moderate or large surface superheats, vapor fragments are found to depart from the foam cover continuously.
3. Copper foams could decrease the surface superheat and eliminate the temperature excursion at boiling incipience.
4. Three distinct heat transfer regions are identified. Region I and II are those of liquid natural convection heat transfer, and nucleate boiling heat transfer for all the ppi foams. Region III is that of either the resistance to vapor release for the 30 and 60 ppi foam covers, or the capillary-assist liquid flow towards foam cells for the 90 ppi foam covers.
5. Boiling curves have different slopes in the three regions. Crossover of boiling curves is found between the 90 ppi and low ppi foam covers.
6. The value of ppi has an important effect on heat transfer performance. Larger value of ppi with small pore size has larger resistance to vapor release, lowering the heat transfer performance at small or moderate surface superheats. However, it has larger capability for liquid suction towards foam cells at high surface superheats, leading to the improved heat transfer performance and extended range of surface superheats. This is the major reason for the crossover of boiling curves between high and low ppi foam covers.
7. Heat transfer coefficients behave the quasi-parabola distribution, with the increased, maximum and then decreased values with continuous increases in heat fluxes, except for the 90 ppi foam covers. The 90 ppi foam covers almost do not change heat transfer coefficients after they attain the maximum value.
8. Larger foam cover thickness enhances nucleate boiling heat transfer due to the increased bubble nucleation site density in region II, but decreases heat transfer performance due to the increased resistance to vapor release in region III.
9. Higher pool liquid temperature enhances nucleate boiling heat transfer in region II. But pool liquid temperatures have small effect on the heat transfer performance in region III.

Acknowledgements

This paper is supported by the National Basic Research Program (2006CB601203) and the National Natural Science Foundation of China (50776089).

References

Arbelaez, F., Sett, S., Mahajan, R.L., 2000. An experimental study on pool boiling of saturated FC-72 in highly porous aluminum metal foams. In: 34th National Heat Transfer Conference, Pittsburgh, Pennsylvania, August 20–22.

Athreya, B.P., Mahajan, R.L., Sett S., 2002. Pool boiling of FC-72 over metal foams: effect of foam orientation and geometry. In: 8th AIAA/ASME Joint Thermophysics and Heat Transfer Conference, St. Louis, Missouri, June 24–26.

Calmidi, V.V., 1998. Transport Phenomenon in High Porosity Metal Foams, Ph.D. Thesis. University of Colorado, CO, USA.

Chen, Y., Groll, M., Mertz, R., Kulenovic, R., 2005. Visualization and mechanisms of pool boiling of propane, isobutane and their mixtures on enhanced tubes with reentrant channels. Int. J. Heat Mass Transfer 48, 2516–2528.

Coursey, J.S., Kim, J., Boudreaux, P.J., 2005. Performance of graphite foam evaporator for use in thermal management. J. Electron. Packag. 127, 127–134.

Ghiu, C.D., Joshi, Y.K., 2005. Visualization study of pool boiling from thin confined enhanced structures. Int. J. Heat Mass Transfer 48, 4287–4299.

Honda, H., Wei, J.J., 2004. Enhancement boiling heat transfer from electronic components by use of surface microstructures. Exp. Thermal Fluid Sci. 28, 159–169.

Kim, J.H., Rainey, K.N., You, S.M., Pak, J.Y., 2002. Mechanism of nucleate boiling heat transfer enhancement from microporous surfaces in saturated FC-72. J. Heat Transfer ASME 124, 500–506.

Kretschmer, C.B., Nowakowska, J., Wiebe, R., 1946. Solubility of oxygen and nitrogen in organic solvents from −25 °C to 50 °C. Ind. Eng. Chem. 38, 506–509.

Liter, S.G., Kaviany, M., 2001. Pool boiling CHF enhancement by modulated porous-layer coating: theory and experiment. Int. J. Heat Mass Transfer 44, 4287–4311.

Meléndez, E., Reyes, R., 2006. The pool boiling heat transfer enhancement from experiments with binary mixtures and porous heating covers. Exp. Thermal Fluid Sci. 30, 185–192.

Moghaddam S., Ohadi M., 2003. Pool boiling of water and FC-72 on copper and graphite foams. In: Proceedings of ASME InterPACK'3, International Electronic Packaging Technical Conference and Exhibition, Maui, Hawaii, July 6–11.

Nimkar, N.M., Bhavnani, S.H., Jaeger, R.C., 2006. Effect of nucleation site spacing on the pool boiling characteristics of a structure surface. Int. J. Heat Mass Transfer 49, 2829–2839.

Parker, J.L., El-Genk, M.S., 2005. Enhanced saturation and subcooled boiling of FC-72 dielectric liquid. Int. J. Heat Mass Transfer 48, 3736–3752.

Rainey, K.N., You, S.M., 2000. Pool boiling heat transfer from plain and microporous, square pin-finned surfaces in saturated FC-72. J. Heat Transfer ASME 122, 509–516.

Wei, J.J., Honda, H., 2003. Effects of fin geometry on boiling heat transfer from silicon chips with micro-pin-fins immersed in FC-72. Int. J. Heat Mass Transfer 46, 4059–4070.

Yaws, C.L., 1999. Chemical Properties Handbook. Mcgraw-Hill, New York.